Role of dynamic effects in the characterization of multilayers by means of power spectral density

Anton Haase,* Victor Soltwisch, Christian Laubis, and Frank Scholze

Physikalisch-Technische Bundesanstalt (PTB), Abbestr. 2-12, 10587 Berlin, Germany

*Corresponding author: anton.haase@ptb.de

Received 6 January 2014; revised 24 March 2014; accepted 4 April 2014;
posted 8 April 2014 (Doc. ID 203389); published 0 MONTH 0000

In this paper, we present measurements of angle- and wavelength-resolved diffuse scattering of EUV radiation on a Mo/Si multilayer. Our sample is optimized for high reflectivity at 13.5 nm wavelength near-normal incidence. We present a rigorous theoretical analysis of the off-specular EUV scattering on the basis of the distorted-wave Born approximation. We prove that the determination of the interface roughness power spectral density (PSD) is only possible by considering geometry-dependent and dynamic contributions. The scattering from multilayer mirrors leads to an intrinsic enhancement in off-specular intensity independent of roughness properties. The thickness oscillations in the scattering intensity (Kiessig fringes) are found to cause additional dynamic enhancement in analogy to Bragg-like peaks for grazing incidence geometry. Considering these effects, the interface PSD is consistently determined.

OCIS codes: (340.7480) X-rays, soft x-rays, extreme ultraviolet (EUV); (290.5880) Scattering, rough surfaces; (120.5820) Scattering measurements.

http://dx.doi.org/10.1364/AO.99.099999

1. Introduction

Multilayer systems have been of great interest over the past decades. The first applications of multilayers serving as mirrors for soft x rays were optical components for space probes. The main driving force today is the shift in direction toward the EUV spectral range at 13.5 nm wavelength in optical lithography for the semiconductor industry. Lenses in classic lithography systems are replaced by multilayer mirrors. High reflectivities are achieved by utilizing the constructive interference of the reflected light at each interface when fulfilling the Bragg condition. State-of-the-art Mo/Si multilayer mirrors reach reflectivities of up to 70% [1,2] in the case of near-normal incidence EUV radiation. This value is still well below the theoretical limit of approximately 75% for an ideal multilayer. An important reason for the loss of reflectivity is interface imperfections such as roughness and interdiffusion causing diffuse scattering. The analysis of the off-specular scattering thus serves as a natural tool for the characterization of interfacial roughness.

At the Physikalisch–Technische Bundesanstalt (PTB), angle- and energy-resolved scatterometric measurements have been performed to analyze the off-specular scattering using EUV radiation. The tunability of synchrotron radiation in conjunction with angular resolution allows obtaining 2D intensity maps close to the relevant multilayer resonance for near-normal incidence geometries. The diffuse scattering from interface roughness contains information on its morphology, such as lateral and vertical correlations, its jaggedness, and mean amplitude. A rigorous analysis of the reciprocal space represented through the scattering pattern; thus it provides access to the interface morphology.

Scatterometry poses an inverse problem of gaining information about the properties of the interfaces. A theoretical model of the diffuse scattering is required to yield a reconstruction of the actual sample and

1559-128X/14/130001-01$15.00/0

deduct the power spectral density (PSD) of roughness. The topic of experimental and theoretical analysis toward the characterization of roughness involving optical wavelengths has been largely studied by others and published in the optical community [3–8]. We take a different approach involving the analysis of diffuse EUV scattering employing numerical simulations of the expected scattering distribution based on the distorted-wave Born approximation (DWBA) [9,10].

We will show that a rigorous, dynamic calculation of the EUV radiation interacting with the multilayer is required to obtain the power spectral densities. The influence of multiple reflections at the layer boundaries cannot be neglected in this analysis. The simulations are compared to measured data obtained for high-reflectance Mo/Si multilayers. The influence of the measurement geometry of the diffuse scattering is discussed in detail.

2. Experimental Methods

The experiments were conducted at the soft x ray radiometry beamline of the PTB laboratory [11]. It is located at the electron storage ring for synchrotron radiation BESSY II in Berlin-Adlershof. The beamline offers a tunable spectral range from 0.7 to 35 nm in combination with a highly collimated photon beam [12]. The total collimation at the experimental station is below 200 μrad, while the scatter halo of the beam is suppressed to below 10^{-5} relative intensity within 1.7 mrad with respect to the center of the beam.

The measurements were performed using angle- and energy-resolved scatterometry. The experimental station is contained in a vacuum chamber allowing measurements at pressures below 10^{-7} mbar. The sample holder is placed on a goniometer [13]. The scatter intensities presented in this study were recorded in the reflection plane using a GaAsP photodiode. This setup offers a wide angular range for specular and off-specular measurements.

The sample used in the experiments is a high-reflectance multilayer with 68.5(7)% reflectivity at an angle of incidence of $\alpha_i = 6.75°$ and a wavelength of 13.5 nm. The silicon substrate was coated with a multilayer stack of molybdenum (Mo) and silicon (Si) with B_4 C and carbon interdiffusion layers with a number of periods of 65. It was fabricated using magnetron sputtering at the Frauenhofer IWS, Dresden [1]. To determine the composition of the multilayer, the reflectivity was measured in a wavelength range of 10 to 16 nm.

In order to gain information on interfacial roughness, the off-specular scattering of the multilayer sample was measured in different geometries. We performed coplanar rocking and detector scans as shown in Fig. 1. The corresponding paths through reciprocal space are different for these two cases. They are shown schematically in Fig. 2. In addition, a wavelength scan (λ scan) was performed at each angular position. By changing the wavelength and the

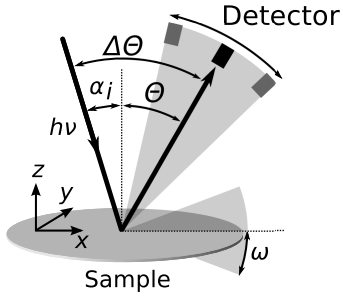

Fig. 1. Coplanar measurement geometries. By keeping the opening angle ΔΘ between incident and exit beam and the detector fixed, respectively, a rocking scan can be performed by changing the sample angle ω. In a detector scan, the sample angle ω is kept fixed and defines the angle of incidence while the detector is moved along Θ.

angle in the same measurement, both degrees of freedom (q_x and q_z) in reciprocal space become accessible. Following this method, we recorded 2D reciprocal space maps of the vicinity of the first Bragg resonance. The reciprocal space coordinates in terms of the experimental parameters are given by

$$q_x = \frac{2\pi}{\lambda}(\sin(\Theta) - \sin(\alpha_i)), \quad (1)$$

$$q_z = \frac{2\pi}{\lambda}(\cos(\Theta) + \cos(\alpha_i)), \quad (2)$$

where λ is the wavelength of the incoming light, Θ is the exit angle with respect to the surface normal (detector angle), and α_i is the angle of incidence with respect to the surface normal.

A. Reciprocal Space Maps for Different Measurement Geometries

The reciprocal space maps in Fig. 3 for the rocking scan (b) at an opening angle of $\Delta\Theta = 13.5°$ and the rocking scan (c) at an opening angle of $\Delta\Theta = 30°$ (corresponding to an angle of incidence of $\alpha_i = 6.75°$ and $\alpha_i = 15.0°$, respectively, in specular geometry) and for the detector scan with the angle of incidence $\alpha_i = 6.75°$ clearly show different symmetries. We observe a strong enhancement in the off-specular scattering

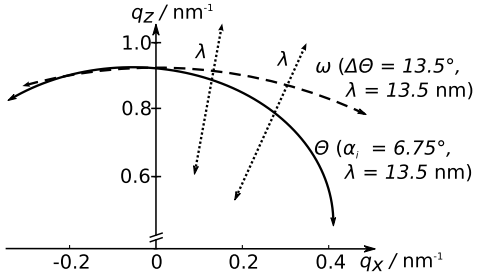

Fig. 2. Schematic positions in reciprocal space in dependence on the measurement geometry. The dashed path represents a rocking scan with the angle ω. The solid line shows the movement in q space when changing the detector angle Θ at a fixed angle of incidence. By tuning the wavelength at each angular position, the q_z direction becomes accessible as indicated by the dotted arrows.

around $q_x \approx 0.1$ nm^{-1} [cf. Figs. 3(a) and 3(c)], which is not replicated on the negative q_x axis in case of (a). The rocking scans (b) and (c) are symmetric with respect to the specular axis at $q_x = 0$; however, no enhanced scattering appears in (b). The latter map shows a triangular-shaped intensity distribution for both the positive and negative q_x range. A minimum in width with respect to the q_z direction can be observed here around $q_x \approx \pm 0.2$ nm^{-1}. The triangular shape also appears for the positive q_x range of the detector scan in Fig. 3(a), where the minimum in width coincides with the intensity maximum.

In Fig. 4, the three measurements shown above are compared by considering the intensity distribution along $q_z = 0.93$ nm^{-1}, which corresponds to the momentum transfer at the multilayer resonance. The differences in the off-specular scattering are evident.

The measurement geometry dependence of the reciprocal space maps indicates that the intensity distributions cannot be the result of multilayer roughness properties alone, i.e., the PSD. Scattering intensities caused by roughness occur at identical positions in reciprocal space for any measurement geometry. In order to explain the observations shown here, the proper theoretical description of the diffuse scattering distributions is presented in the following section.

3. Theoretical Background

Our theoretical description of the diffuse EUV scattering from multilayers is based on the DWBA [9,10], which is widely used in the analysis of hard x-ray

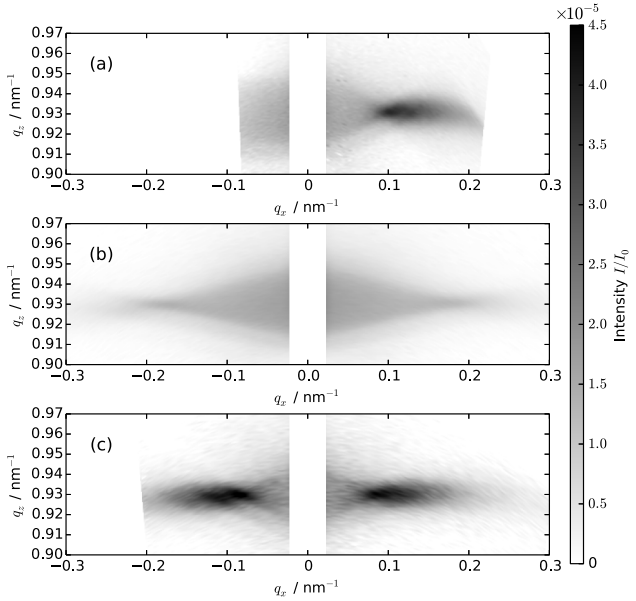

F3:1 Fig. 3. (a) Measured intensity map of a detector scan of a Mo/Si
F3:2 multilayer mirror at an angle of incidence $\alpha_i = 6.75°$. (b) Measured
F3:3 intensity maps of the identical sample obtained through rocking
F3:4 scans at an opening angle between detector and incident beam
F3:5 of $\Delta\Theta = 13.5°$ and (c) $\Delta\Theta = 30°$. The area close to the specular axis
F3:6 was excluded from this dataset due to its strong intensity com-
F3:7 pared with the diffuse scattering shown here. The access to the
F3:8 negative q_x axis in (a) is limited due clipping of the incoming beam
F3:9 with the detector.

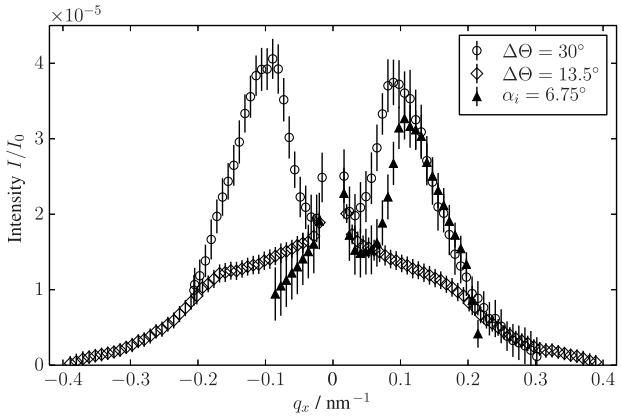

F4:1 Fig. 4. Averaged diffuse scattering intensity along q_x in the inter-
F4:2 val $q_z = (0.930 \pm 0.003)$ nm^{-1} corresponding to the resonance of
F4:3 the multilayer. The data shown are two rocking scan and one de-
F4:4 tector scan geometries (see text for details).

scattering. The DWBA is a perturbation theory in which the interfacial roughness is considered to be a small deviation from the ideal multilayer. This corresponds to a potential in the wave equation

$$(\Delta + K^2)|E(\mathbf{r})\rangle = V(\mathbf{r})|E(\mathbf{r})\rangle \tag{3}$$

of $V(\mathbf{r}) = V_{\mathrm{id}}(\mathbf{r}) + V_r(\mathbf{r})$ that can be separated into a strong part $V_{\mathrm{id}}(\mathbf{r})$ for which an analytical solution exists and a small perturbation $V_r(\mathbf{r})$ describing the interfacial roughness. In case of a multilayer, we start from the dynamic calculation of the electric fields of a perfectly flat multilayer. The wave equation [Eq. (3)] is solved by calculating the field amplitudes using a matrix formalism [14].

For the calculation of the specular reflectivity curve, it is necessary to correct the field calculation for the interfacial roughness and diffusion. Modified Fresnel coefficients according to Névot/Croece [15] assuming a Gaussian interface profile are used:

$$r^{(j)} = r_{\mathrm{id}}^{(j)} \exp(-2k_z^{(j)}k_z^{(j+1)}\sigma_j^2), \tag{4}$$

$$t^{(j)} = t_{\mathrm{id}}^{(j)} \exp((k_z^{(j)} - k_z^{(j+1)})^2\sigma_j^2/2), \tag{5}$$

where $r_{\mathrm{id}}^{(j)}$ and $t_{\mathrm{id}}^{(j)}$ are the Fresnel reflection and transmission coefficients, respectively, for the ideal jth interface, σ_j is the root mean square roughness (rms) and $k_z^{(j)}$ is the z component of the incidence wave vector at the jth interface.

The diffuse scattering cross section is given by the covariance of the matrix element of the perturbation potential on the basis of the wave functions from the analytic solution for a given incidence and exit angle [9,16]

$$\left(\frac{d\sigma}{d\Omega}\right)_{\mathrm{diffuse}} = \mathrm{Cov}(\langle E_{\mathrm{id},1}|V_r|E_{\mathrm{id},2}\rangle), \tag{6}$$

where $|E_{\mathrm{id},i}\rangle, i = 1, 2$ are the solutions of the wave equation [Eq. (3)] for the ideal multilayer and the

given incidence and exit angles, respectively, calculated using the unmodified Fresnel coefficients $r_{\mathrm{id}}^{(j)}$ and $t_{\mathrm{id}}^{(j)}$ representing the perfectly flat multilayer. Since the roughness potential is nonzero only at the individual interfaces, Eq. (6) can be decomposed into a sum over the matrix elements at each interface j. In the following, we use the small roughness $q_{z,j}\sigma_j \ll 1$ approximation, which is valid for any high-quality multilayer mirror (cf. [17] for the more general expression).

In the case of small reflectivity amplitudes, dynamic multiple reflections are often neglected, and the dominant term in the decomposition is diffuse scattering of the transmitted fields at the roughness of each interface. The so-called semi-kinematic approximation [16] yields an explicit expression for Eq. (6) with

$$\left(\frac{d\sigma}{d\Omega}\right)_{\text{diffuse}}^{\text{semi-kinematic}} = \frac{A\pi^2}{\lambda^4}\sum_{j=1}^{N}\sum_{i=1}^{N}((n_j^2 - n_{j+1}^2)^*(n_i^2 - n_{i+1}^2) \times T_j^{(1)*}T_j^{(2)*}T_i^{(1)}T_i^{(2)}S_{ij}(q_x)), \tag{7}$$

where A is the illuminated sample area, λ the wavelength of the incident light, and n_j is the complex index of refraction of material j. The $T_j^{(1,2)}$ are defined as the amplitude of the transmitted field at the interface j for the given exit angle (2) (represented as a time-inverted beam originating at the detector) and incidence angle (1). The total field at the jth interface is expressed in terms of the reflected field $E_r^{(j)}(z)$ propagating toward the vacuum and the transmitted field $E_t^{(j)}(z)$ propagating toward the substrate

$$E_t^{(j)}(z) = T_j e^{ik_z(j)z}, \tag{8}$$

$$E_r^{(j)}(z) = R_j e^{-ik_z(j)z} \tag{9}$$

with $E_{\mathrm{id}}^{(j)}(\mathbf{r}) = e^{i\mathbf{k}_\parallel\mathbf{r}_\parallel}(E_t^{(j)}(z) + E_r^{(j)}(z))$ being the full solution of the wave equation Eq. (3) for the ideal multilayer at the jth interface. $S_{ij}(q_x)$ is the structure factor describing the influence of the interfacial roughness on the diffuse scattering intensity defined through

$$S_{ij}(\vec{q}_\parallel; q_z^{(j)}, q_z^{(i)}) = \frac{\exp[-((q_z^{(j)*})^2\sigma_j^2 + (q_z^{(i)})^2\sigma_i^2)/2]}{q_z^{(j)*}q_z^{(i)}} \times \int \mathrm{d}^2\vec{X}(\exp[q_z^{(j)*}q_z^{(i)}C_{ij}(\vec{X})] - 1) \times \exp(i\vec{q}_\parallel\cdot\vec{X}), \tag{10}$$

where $q_z^{(i)}$ is the z component of the scattering vector $\vec{q}$ at the ith interface, $\vec{X} = \vec{x} - \vec{x}'$ is the lateral distance vector, and $C_{ij}(\vec{x} - \vec{x}') = \langle h_i(\vec{x})h_j(\vec{x}')\rangle$ is the correlation function of the interface profiles $h(\vec{x})$ of the interfaces i and j [17,18]. In case of the small roughness approximation,

$$\frac{\exp[-((q_z^{(j)*})^2\sigma_j^2 + (q_z^{(i)})^2\sigma_i^2)/2]}{q_z^{(j)*}q_z^{(i)}} \approx \frac{1}{q_z^{(j)*}q_z^{(i)}} \tag{11}$$

and $\exp[q_z^{(j)*}q_z^{(i)}C_{ij}(\vec{X})] - 1 \approx q_z^{(j)*}q_z^{(i)}C_{ij}(\vec{X})$ apply and Eq. (10) reduces to

$$S_{ij}(\vec{q}_\parallel) \approx \int \mathrm{d}^2\vec{X}C_{ij}(\vec{X})\exp(i\vec{q}_\parallel\cdot\vec{X}). \tag{12}$$

$S_{ij}(\vec{q}_\parallel)$ is, thus, the Fourier transform of the correlation function $C_{ij}(\vec{X})$. In case of coplanar scattering, furthermore $\vec{q}_\parallel \equiv \vec{q}_x$. Assuming identical growth for the individual layers, i.e., a material independent propagation of roughness along the z direction, $S_{ij}(q_x)$ can be expressed in terms of the lateral PSD $C_i(q_x)$ and a vertical replication factor $c_{ij}^{\perp}(q_x)$ [19],

$$S_{ij}(q_x) = c_{ij}^{\perp}(q_x)C_{\max(i,j)}(q_x). \tag{13}$$

Other PSD functions based on different models of lateral interface roughness correlation have been proposed, e.g., by Sinha *et al.* [16]. We follow the approach by de Boer and co-workers [18,20] for fractal interface roughness, where the lateral correlation function of the ith interface is given by

$$\tilde{C}_i(\vec{X}) = P_i\xi_\parallel^{H_i}|\vec{X}|^{H_i}K_{H_i}(|\vec{X}|/\xi_\parallel). \tag{14}$$

H_i is the Hurst factor providing a measure for the jaggedness of the interface [16], K_{H_i} are the modified Bessel functions of the order H_i, $\xi_\parallel$ is a lateral correlation length, and

$$P_i = \frac{\sigma_i^2}{\xi_\parallel^{H_i-1}2^{H_i-1}\Gamma(1+H_i)/H_i}. \tag{15}$$

Our goal is to determine a single average PSD. We thus do not distinguish between individual interfaces in the model and assume an identical roughness properties for all interfaces. Hence $\sigma_j = \sigma$, $H_j = H$ and $C_{\max(i,j)}(q_x) = C(q_x)$. The PSD is given by the Fourier transform of Eq. (14) with respect to q_x, which yields the closed analytic form

$$C(q_x) = \frac{4\pi H\sigma^2\xi_\parallel^2}{(1+|q_x|^2\xi_\parallel^2)^{1+H}}. \tag{16}$$

The high degree of thickness stability for well-defined multilayers as is necessary for high-performance mirrors implies a high degree of vertical correlation of individual interfaces roughness throughout the stack. In order to derive the replication factor in Eq. (13), we follow Stearns [21]. In this

model, the evolution of the surface roughness $w(x,y)$ during the growth of a single layer is described by the Langevin equation. In its Fourier transformed form,

$$\frac{\partial w(f)}{\partial t} = -4\pi^2 v f^2 w(f) + \frac{\partial \eta(f)}{\partial t}, \tag{17}$$

where v is a diffusion-like parameter, $\eta(f)$ is random noise normalized to the layer thickness, and $w(f)$ describes the roughness evolution in dependence of the spacial frequency f. The roughness evolution during the growth of a single layer of a specific material can then be evaluated by discritizing Eq. (17) for the successive deposition of material of thickness δd

$$w_i(f) = c_\perp(f;\delta d) w_{i-1}(f) + \eta(f), \tag{18}$$

where $c_\perp(f;\delta d)$ is the replication factor of roughness for a single deposition. In the limit of repeated infinitesimal depositions until the full nth layer of thickness d_n is grown, $c_\perp(f,d_n)$ can be evaluated to be [19]

$$c_\perp(f,d_n) = \exp(-4\pi^2 f^2 v d_n) = \exp(-q_x^2 v d_n) \tag{19}$$

with $q_x^2 = 4\pi^2 f^2$. Assuming identical diffusionlike behavior v for all materials of a multilayer and defining $\xi_\perp(q_x) = 1/(v q_x^2)$, the replication factor in Eq. (13) is given by

$$c_{ij}^{\perp}(q_x) = \exp\left(-\sum_{n=\min(i,j)}^{\max(i,j)-1} d_n/\xi_\perp(q_x)\right). \tag{20}$$

Here, $\xi_\perp(q_x)$ can be interpreted as a frequency-dependent vertical correlation length, describing the distance perpendicular to the stack until the replication factor decreased to $1/e$.

Gullikson and Stearns [22] observed that the direction of the vertical replication of roughness can be tilted with respect to the surface normal. This leads to tilted Bragg planes requiring a coordinate transformation in reciprocal space to account for the tilt angle β according to

$$\bar{q}_z = q_z - q_x \tan\beta. \tag{21}$$

Since, the vertical scattering vector components enter the calculations through the Fresnel coefficients $r_{\mathrm{id}}^{(j)}$ and $t_{\mathrm{id}}^{(j)}$, an additional factor enters the calculation of Eq. (13) through substitution by

$$\bar{S}_{ij}(q_x) = \exp(-iq_x \tan\beta(z_i - z_j)) S_{ij}(q_x), \tag{22}$$

where z_i is the z position of the ith interface.

So far, multiple reflections at the interfaces have been ignored (semi-kinematic approximation). However, in the case of high-reflectance multilayer mirrors, this might not be valid. In order to include first-order multiple reflections, i.e., single reflection and transmission processes before and after the diffuse scattering event, in the theoretical treatment, the reflected fields need to be included in Eq. (6). The explicit expression considering dynamic multiple reflections within the layer is given by

$$\left(\frac{d\sigma}{d\Omega}\right)_{\mathrm{diffuse}}^{\mathrm{dynamic}} = \left[\frac{A\pi^2}{\lambda^4}\sum_{j=1}^{N}\sum_{i=1}^{N}(n_j^2 - n_{j+1}^2)^*(n_i^2 - n_{i+1}^2) \times ((T_j^{(1)} + R_j^{(1)})^*(T_j^{(2)} + R_j^{(2)})^* \times (T_i^{(1)} + R_i^{(1)})(T_i^{(2)} + R_i^{(2)}))c_\perp^{ij}\right] C(q_x), \tag{23}$$

where $R_j^{(1,2)}$ are the reflected field amplitude at interface j for the given incidence angle (1) and exit angle (2), the latter again in a time-inverted representation of a beam originating at the detector.

4. Numerical Simulations

We have applied the theory above to the multilayer in our experiments. In order to obtain a model for the layer thicknesses in our multilayer, we measured the reflectivity of the sample in dependence on the wavelength. The recorded curve was fitted using the numerical calculation of the reflectivity curve based on the specular fields including the modified Fresnel coefficients in Eqs. (4) and (5). The resulting fit parameters were, then, further used to model the multilayer in the numerical simulations below. The fit of the reflectivity curve was later simultaneously optimized during the fit of the diffuse scattering in order to correct for the change in the mean roughness σ. The final thicknesses in the stack were fitted to $d_{\mathrm{Mo}} = 2.0181$ nm, $d_{B_4C} = 1.3215$ nm, $d_{\mathrm{Si}} = 3.0388$ nm, and $d_C = 0.5858$ nm. The DWBA was implemented in the *Python* programming language using a highly parallel algorithm.

A. Dynamic Contributions to the Diffuse Scattering

In order to determine the contribution of dynamic multiple reflections within the stack, we compared the semi-kinematic approximation in Eq. (7) with the dynamic calculations in Eq. (23). For this comparison, we simulated a rocking scan at an opening angle of $\Delta\Theta = 30°$ and compared the simulations with the measured data. The roughness properties for these simulations were determined following the procedure described below in Section 4.C, including a discussion on the influence of the parameters, specifically $\xi_\perp(q_x)$, on these vertical line cuts.

A quantitative comparison of the dynamic contribution to the total scattering intensity in our measurements is shown in Fig. 5 as a line cut along q_z at $q_x = 0.05$ nm^{-1}. The dynamic calculation yields excellent agreement with the measured data. The results show distinct differences with an increase up to 100% of the scattered intensity close to the multilayer resonance at $q_z = 0.93$ nm^{-1} compared to the semi-kinematic calculation. Hence, dynamic contributions are dominant in the vicinity of the Bragg resonance.

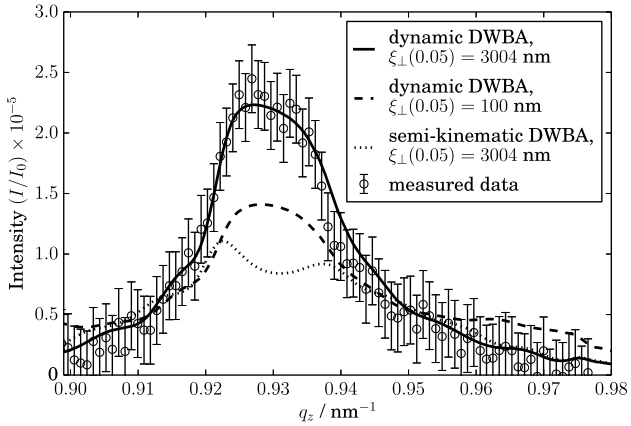

F5:1 Fig. 5. Scattering intensity along q_z for $q_x = 0.05$ nm^{-1} for the
F5:2 dynamic and semi-kinematic calculations for a rocking scan at
F5:3 $\Delta\Theta = 30°$ in comparison to the measured data.

To evaluate the contribution of multiple reflections due to the subsidiary maxima, Fig. 6 shows the intensity distribution along q_x at $q_z = 0.93$ nm^{-1}. These maxima are caused by interference of the reflections from the top surface of the multilayer stack and the substrate interface (Kiessig fringes) [23]. The solid line corresponds to the dynamic theory, while the dotted line is the result of the semi-kinematic calculation. The dashed vertical lines indicate the limits of the main Bragg peak. These positions are defined through the first minimum on each side of the reflectivity peak (cf. inset in Fig. 6). The vertical red lines show the position of multiple reflections due to Kiessig fringes close to the main resonance. Again, the corresponding positions in the specular reflectivity measurement are shown in the inset. Each of the marked fringes appears on the negative and positive q_x axis in the main plot. This is caused by the incidence and exit angle, respectively, being at the resonance angle of the various Kiessig maxima in the reflectivity curve. Thus a strong increase with respect to the semi-kinematic approximation is observed. The position of the dynamic contribution from the first Kiessig fringes on either side of the main resonance exhibits a pronounced maximum in the diffuse scattering. These fringes contribute most due to their high overall relative intensity compared with the fringes further away from the reflectivity maximum. In addition, the position in reciprocal space coincides with the first two Kiessig fringes marked on either side of the main maximum. This effect of dynamic maxima is similar to the observation of Bragg-like peaks in grazing incidence geometry [24], but it is caused by the subsidiary maxima instead. Consequently, we name this enhancement "Kiessig-like peaks." The contribution by the main Bragg resonance similar to the observations in Fig. 5 amounts to approximately 100% at $q_x = 0$.

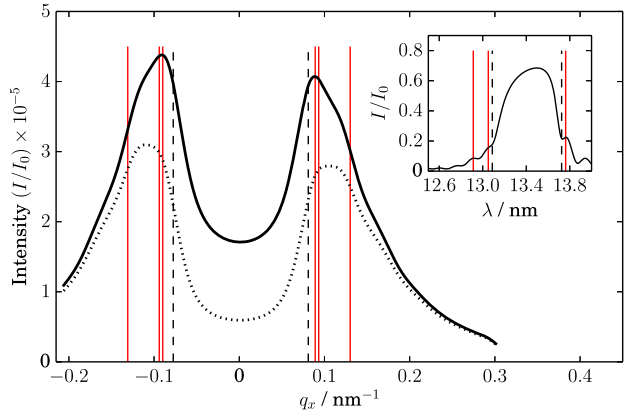

F6:1 Fig. 6. Scattering intensity distribution at $q_z = 0.93$ nm^{-1}. The
F6:2 solid line shows the result of the dynamic calculation for a rocking
F6:3 scan with an opening angle of $\Delta\Theta = 30°$. The dashed line repre-
F6:4 sents the calculation applying the semi-kinematic approximation,
F6:5 ignoring any multiple reflections within the multilayer. The
F6:6 dashed vertical lines are the limits of the main Bragg peak, while
F6:7 the red solid vertical lines show the position of dynamic contribu-
F6:8 tions of the Kiessig fringes close to the main maximum. Each
F6:9 Kiessig fringe marked in the inset appears for the corresponding
F6:10 positive and negative q_x value. The strong intensity at $q_x \approx$
F6:11 0.1 nm^{-1} results from the overlap of the dynamic maxima of
F6:12 two different Kiessig fringes (see text).

B. Multilayer Enhancement Factor

The total contribution of the multilayer to the diffuse scattering, independent of lateral interface roughness properties, is described by the sum in the square brackets of Eq. (23) as a prefactor to the PSD $C(q_x)$. It describes the modulation of the scattering intensity due to the multilayer nature of the scattering structure, independent of the interface roughness. We thus consider it as a "relative multilayer enhancement factor." The result of the calculations based on the layer model of our multilayer sample is shown in Fig. 7 for one detector and two rocking scan configurations. The vertical correlation length for this specific multilayer mirror is $\xi_\perp(q_x) = 7.5/q_x^2$ nm^{-1} as expected for a high-reflectance mirror, where $\xi_\perp$ exceeds the total thickness D of the entire stack for $|q_x| < 0.12$ nm^{-1}. The method for the extraction of the vertical correlation length from the measured data is discussed in Section 4.C. The multilayer

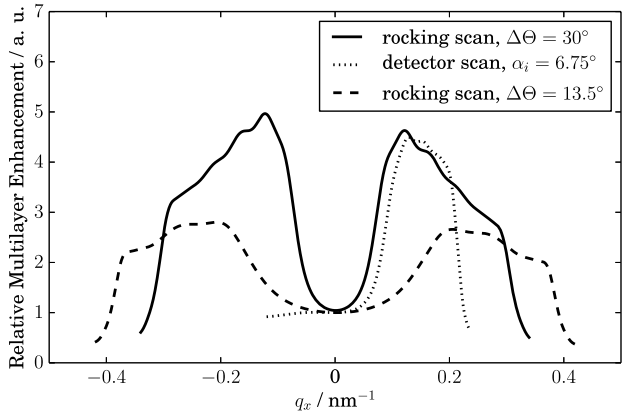

F7:1 Fig. 7. Enhancement factor due to the specific properties of mul-
F7:2 tilayer reflectivity for three different measurement geometries.
F7:3 The simulations shown here were normalized with respect to
F7:4 the diffuse contribution to the specular reflectivity at $q_x = 0$.

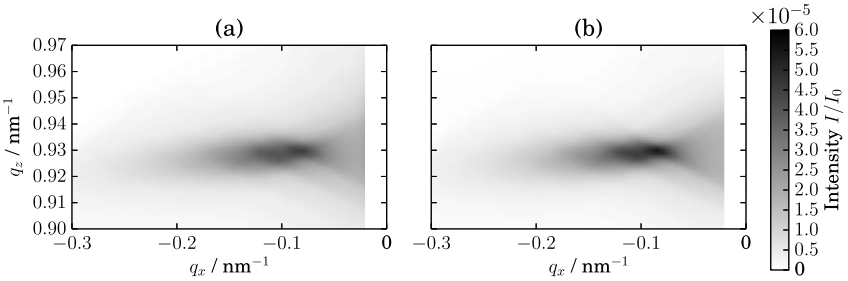

F8:1 Fig. 8. Measured (a) and simulated (b) reciprocal space maps for a rocking scan at an opening angle of $\Delta\Theta = 30°$ with the roughness
F8:2 parameters determined in Section 4.C.

enhancement factor was normalized with respect to $q_x = 0$, i.e., the calculated diffuse scattering contribution on the specular axis.

The results clearly show that diffuse scattering from multilayers at near-normal incidence exhibit strong enhancement due to the intrinsically limited bandpass of reflectivity of multilayers. If both the incidence and exit angles are out of the Bragg resonance, the higher penetration depth of the multilayer causes an increase in the number of interfaces contributing to the diffuse scattering intensity. Thus higher total scattering is observed. The Kiessig fringes cause modulations in the enhancement factor increased by the purely dynamic processes described in Section 4.A.

C. Reconstruction of the Power Spectral Density

In order to extract roughness properties from the off-specular measurements shown above, a correction for the influence of the multilayer as discussed in Section 4.B is required. The scattering intensity after division by the multilayer enhancement factor represents the PSD of roughness. The measured PSDs are shown in Fig. 9 for all three experiments. The excellent agreement with each other within the uncertainty margin confirms the validity and necessity of the dynamic theory to model the diffuse scattering from the multilayer. The reconstruction of the parameters of the PSD in Eq. (16) can be done by considering the overall intensity as well as the asymptotic behavior [25] of the measured data in Fig. 9.

The numerical simulations show a strong sensitivity with respect to the mean roughness parameter σ through the total portion of diffusely scattered light. As expected for a high-reflectance mirror, we obtained a small roughness value of $\sigma = 0.2$ nm.

It follows from the definition of the PSD in Eq. (16) that the lateral correlation length $\xi_\parallel$ defines a cut-off for the spatial frequencies contributing to the off-specular scattering. We performed several simulations to compare the simulated intensity profile with the cut-off frequency observed in the measured data. A correlation length of $\xi_\parallel = 5.6$ nm was obtained following this method. The fractal nature of the interfaces was analyzed by varying the Hurst parameter H. The asymptotic behavior of the PSD for $q_x > 10^{-1}$ nm^{-1} for the multilayer sample measured yields a Hurst factor of $H = 1.0$, which corresponds to a smooth roughness profile [16]. By following this procedure, measurements of power spectral densities are possible, independent of the measurement geometry.

For a full characterization of the multilayer, the determination of the vertical correlation length remains. This parameter is also accessible through the 2D reciprocal space maps. It has been observed elsewhere that the vertical correlation of the interfacial roughness leads to resonant diffuse scattering ("Bragg sheets") [9]. The width of these sheets with respect to the q_z axis provides a measure for the vertical correlation lengths, e.g., in GISAXS [26]. We observe a similar dependence of the scattering intensity close to the Bragg resonance along the vertical axis (cf. Fig. 5) with a reduction of the scattering intensity at the resonance for small correlation length but a higher relative scattering intensity far off resonance (cf. $q_z > 0.95$ nm^{-1} in Fig. 5). We varied the vertical correlation length $\xi_\perp(q_x)$ and fitted several vertical cuts of the reciprocal space map simultaneously with the PSD determination. The best model for our sample yields a high vertical correlation length of $\xi_\perp(q_x) = 7.5/q_x^2$ nm^{-1}, as expected for high-reflectance mirrors, at a tilt angle of $\beta = -1°$ of the Bragg plane. This correlation length exceeds the total thickness of the multilayer coating up to

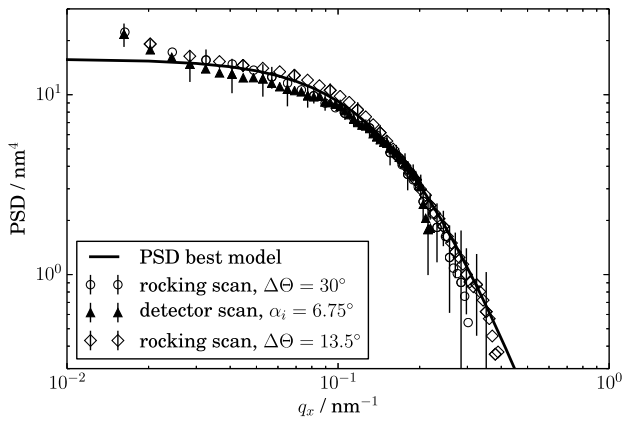

Fig. 9. Diffuse scattering intensity corrected for the multilayer enhancement factor considering a tilt angle of $\beta = -1°$ according to Eq. (22). The black solid line corresponds to a PSD with $\xi_\parallel = 5.6$ nm, $H = 1.0$, and $\sigma = 0.2$ nm and a vertical correlation length of $\xi_\perp(q_x) = 7.5/q_x^2$ nm^{-1}.

$|q_x| < 0.13\ \mathrm{nm}^{-1}$ and thus indicates (almost) full replication of roughness throughout all interfaces for the specified spacial frequencies.

By combining the findings for the properties of roughness in the PSD and the multilayer enhancement factor determined by the layer structure of the multilayer, we are able to fully reconstruct the measured intensity distribution for all geometries. The simulated reciprocal space map for a rocking scan with an opening angle of $\Delta\Theta = 30°$ based on the parameters determined in the previous analysis is shown in Fig. 8(b). The calculation is in excellent agreement with the measured reciprocal space map in Fig. 8(a).

5. Conclusions

We have applied near-normal incidence diffuse scattering in the EUV spectral range to analyze the interfacial roughness of Mo/Si multilayers. At-wavelength reciprocal space maps in the vicinity of the main Bragg resonance of the multilayer were recorded for the first time via angle- and wavelength-resolved scatterometry. We observed intensity enhancements in the off-specular scattering. Experiments in different geometries revealed a dependence of the off-specular scattered intensity on the measurement geometry.

Numerical simulations based on the distorted-wave Born approximation (DWBA) have been performed. The comparison of semi-kinematic simulations with dynamic calculations show that dynamic effects, i.e., multiple reflections at the interfaces, cannot be neglected. The semi-kinematic approach is invalid when either incidence or exit angle fulfill the Bragg condition. In addition, dynamic multiple reflections caused by increased reflectivity due to the Kiessig fringes close to the main Bragg resonance contribute significantly to the off-specular scattering distribution. The simulations show that the limited bandpass reflection property of the multilayer causes the geometry-dependent diffuse scattering in conjunction with the dynamic maxima.

Therefore, in the determination of the interface morphology from coplanar reciprocal space maps, a multilayer enhancement factor has to be considered to extract the PSD. We have applied our model to two different measurement geometries with two different angles of incidence for the specular case. Together with the multilayer composition determined from modeled specular reflectivity curves rigorous simulations of the diffuse scattering intensity caused by the multilayer were possible, in excellent agreement with the measured data. The average lateral PSD could then be extracted with regard to the multilayer enhancement factor equivalently for any measurement geometry. In addition, measurements along the q_z direction provide information on the vertical correlation of interfaces, i.e., the determination of the vertical correlation length.

In conclusion, the consideration of the dynamic effects in the DWBA allows the characterization of the multilayer with respect to its roughness properties. The diffuse scattering measurements corrected for the multilayer enhancement factor provide a measure of the PSD. Thus this method is not restricted to the specific representation of the PSD used in our model. Alternative PSD models have been discussed in the literature [16,27] and are equivalently applicable in the numerical simulations.

References

1. S. Braun, H. Mai, M. Moss, R. Scholz, and A. Leson, "Mo/si multilayers with different barrier layers for applications as extreme ultraviolet mirrors," Jpn. J. Appl. Phys. **41**, 4074–4081 (2002).
2. T. Feigl, S. Yulin, N. Benoit, and N. Kaiser, "{EUV} multilayer optics," Microelectron. Engin. **83**, 703–706 (2006); in *Micro- and Nano-Engineering {MNE} 2005 Proceedings of the 31st International Conference on Micro- and Nano-Engineering*.
3. C. Amra, C. Grèzes-Besset, and L. Bruel, "Comparison of surface and bulk scattering in optical multilayers," Appl. Opt. **32**, 5492–5503 (1993).
4. C. Amra, "Light scattering from multilayer optics. i. tools of investigation," J. Opt. Soc. Am. A **11**, 197–210 (1994).
5. J. M. Elson, J. P. Rahn, and J. M. Bennett, "Light scattering from multilayer optics: comparison of theory and experiment," Appl. Opt. **19**, 669–679 (1980).
6. J. M. Elson, J. P. Rahn, and J. M. Bennett, "Relationship of the total integrated scattering from multilayer-coated optics to angle of incidence, polarization, correlation length, and roughness cross-correlation properties," Appl. Opt. **22**, 3207–3219 (1983).
7. S. Schröder, T. Herffurth, H. Blaschke, and A. Duparré, "Angle-resolved scattering: an effective method for characterizing thin-film coatings," Appl. Opt. **50**, C164–C171 (2011).
8. S. Schröder, D. Unglaub, M. Trost, X. Cheng, J. Zhang, and A. Duparré, "Spectral angle resolved scattering of thin film coatings," Appl. Opt. **53**, A35–A41 (2014).
9. V. Holý and T. Baumbach, "Nonspecular x-ray reflection from rough multilayers," Phys. Rev. B **49**, 10668–10676 (1994).
10. V. Holý, J. Kube ˇna, I. Ohlídal, K. Lischka, and W. Plotz, "X-ray reflection from rough layered systems," Phys. Rev. B **47**, 15896–15903 (1993).
11. B. Beckhoff, A. Gottwald, R. Klein, M. Krumrey, R. Müller, M. Richter, F. Scholze, R. Thornagel, and G. Ulm, "A quarter-century of metrology using synchrotron radiation by ptb in berlin," phys. status solidi (b) **246**, 1415–1434 (2009).
12. F. Scholze, B. Beckhoff, G. Brandt, R. Fliegauf, A. Gottwald, R. Klein, B. Meyer, U. D. Schwarz, R. Thornagel, J. Tuemmler, K. Vogel, J. Weser, and G. Ulm, "High-accuracy euv metrology of ptb using synchrotron radiation," Proc. SPIE **4344**, 402 (2001).
13. J. Tummler, H. Blume, G. Brandt, J. Eden, B. Meyer, H. Scherr, F. Scholz, F. Scholze, and G. Ulm, "Characterization of the ptb euv reflectometry facility for large euvl optical components," Proc. SPIE **5037**, 265–273 (2003).
14. M. Born and E. Wolf, *Principles of Optics*, 3rd ed. (Cambridge University, 1965).
15. P. Croce and L. Névot, "étude des couches minces et des surfaces par réflexion rasante, spéculaire ou diffuse, de rayons x," Rev. Phys. Appl. **11**, 113–125 (1976).
16. S. K. Sinha, E. B. Sirota, S. Garoff, and H. B. Stanley, "X-ray and neutron scattering from rough surfaces," Phys. Rev. B **38**, 2297–2311 (1988).
17. D. K. G. de Boer, "X-ray scattering and x-ray fluorescence from materials with rough interfaces," Phys. Rev. B **53**, 6048–6064 (1996).
18. D. K. G. de Boer, "X-ray reflection and transmission by rough surfaces," Phys. Rev. B **51**, 5297–5305 (1995).
19. E. Spiller, D. Stearns, and M. Krumrey, "Multilayer x-ray mirrors: interfacial roughness, scattering, and image quality," J. Appl. Phys. **74**, 107–118 (1993).
20. D. K. G. de Boer, A. J. G. Leenaers, and W. W. van den Hoogenhof, "Influence of roughness profile on reflectivity

and angle-dependent x-ray fluorescence," J. Phys. III **4**, 1559–1564 (1994).
21. D. G. Stearns, "X-ray scattering from interfacial roughness in multilayer structures," J. Appl. Phys. **71**, 4286–4298 (1992).
22. E. M. Gullikson and D. G. Stearns, "Asymmetric extreme ultraviolet scattering from sputter-deposited multilayers," Phys. Rev. B **59**, 13273–13277 (1999).
23. H. Kiessig, "Interferenz von röntgenstrahlen an dünnen schichten," Ann. Phys. **402**, 769–788 (1931).
24. V. M. Kaganer, S. A. Stepanov, and R. Köhler, "Bragg diffraction peaks in x-ray diffuse scattering from multilayers with rough interfaces," Phys. Rev. B **52**, 16369–16372 (1995).
25. T. Salditt, D. Lott, T. H. Metzger, J. Peisl, G. Vignaud, P. Høghøj, O. Schärpf, P. Hinze, and R. Lauer, "Interfacial roughness and related growth mechanisms in sputtered w/si multilayers," Phys. Rev. B **54**, 5860–5872 (1996).
26. P. Siffalovic, E. Majkova, L. Chitu, M. Jergel, S. Luby, J. Keckes, G. Maier, A. Timmann, S. Roth, T. Tsuru, T. Harada, M. Yamamoto, and U. Heinzmann, "Characterization of mo/si soft x-ray multilayer mirrors by grazing-incidence small-angle x-ray scattering," Vacuum **84**, 19–25 (2009).
27. G. Palasantzas and J. Krim, "Effect of the form of the height-height correlation function on diffuse x-ray scattering from a self-affine surface," Phys. Rev. B **48**, 2873–2877 (1993).

Queries

1. AU: Figure 8 is not cited in order. Please cite it before Fig. 9 in order to maintain its sequential order.

2. AU: Is it necessary to split Ref. [2] into two references? Please check and confirm.